Sensors & Actuators: B. Chemical 446 (2026) 138731

Contents lists available at ScienceDirect

Sensors and Actuators: B. Chemical

journal homepage: www.elsevier.com/locate/snb

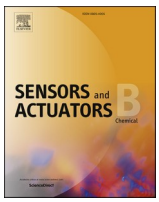

A paper-microfluidic platform for viral RNA and protein detection in saliva for SARS-CoV-2 diagnosis

Yuwei Pan [a,b,1], Xuanye Ma [a,1], Iva Chianella [a], Zhugen Yang [a,*]

[a] Faculty of Engineering and Applied Sciences, Cranfield University, Cranfield MK43 0AL, UK
[b] College of Chemical and Biological Engineering, Zhejiang University, Hangzhou 310058, China

ARTICLE INFO

Keywords:
Paper-microfluidic device
COVID-19
Saliva
Viral RNA
Antibody
Point-of-care testing (POCT)

ABSTRACT

Rapid and sensitive diagnostic methods for infectious diseases are critical for public health management. The reliance of immunoassays on humoral immune responses results in lower detection rates during early infection compared to nucleic acid tests. To address this limitation, we presented a paper-microfluidic platform for rapid and low-cost SARS-CoV-2 diagnosis that simultaneously detected viral RNA and proteins in saliva. The system integrated a streamlined saliva processing protocol, a paper-based colorimetric reverse transcription loop-mediated isothermal amplification (RT-LAMP) assay for viral RNA detection (LOD: 10 copies/μL; Dynamic range: 10–10^7 copies/μL), and a paper-based ELISA (p-ELISA) assay for immunoglobulin titer quantification (LOD: 0.5 ng/μL; Dynamic range: 0.5–60 ng/μL). Lyophilized reagents ensured operational simplicity and long-term stability, while results were interpreted visually or via smartphone imaging. The entire assay was completed within 60 min, with recoveries of 93 %–106 % in saliva samples. By facilitating non-invasive saliva analysis and concurrent assessment of viral load and antibody titers, this platform will provide a comprehensive diagnostic solution, particularly valuable in resource-limited settings.

1. Introduction

Rapid and sensitive diagnosis of infectious diseases is critical for protecting public health [1]. Severe acute respiratory syndrome coronavirus 2 (SARS-CoV-2), the causative agent of coronavirus disease 2019 (COVID-19), has emerged as one of the deadliest viruses in human history since its identification in December 2019 [2–4]. Conventional diagnostic approaches rely on invasive sample collection methods, such as serum or nasopharyngeal swabs [5–7], which pose practical challenges. Recent research highlights saliva as a promising and less invasive alternative for detecting SARS-CoV-2, thereby facilitating the development of saliva-based diagnostic tools for COVID-19 [8–10]. Integrating saliva-derived data with clinical testing could enhance the monitoring of viral transmission dynamics. It's noted that the timely identification of viral nucleic acids and proteins in saliva is pivotal for tracking disease spread and advancing epidemiological research [11–13]. Therefore, there is an increasing demand for rapid, sensitive, and cost-effective diagnostic platforms capable of detecting SARS-CoV-2 nucleic acids and antibodies in saliva samples.

Nucleic acid amplification tests (NAATs) enable rapid and sensitive viral detection, with quantitative reverse transcription polymerase chain reaction (RT-qPCR) serving as the gold-standard method for large-scale COVID-19 diagnosis [14–16]. However, RT-qPCR remains constrained by its reliance on centralized laboratory infrastructure, expensive thermocyclers, and specialized personnel, limiting its applicability for point-of-care testing (POCT) [17]. In contrast, emerging isothermal amplification techniques, such as loop-mediated isothermal amplification (LAMP), offer a cost-effective and user-friendly alternative by facilitating nucleic acid amplification under constant temperature conditions [18–20]. The global rollout of vaccination programs has also highlighted the need for efficient antibody detection and immune monitoring [21]. Enzyme-linked immunosorbent assays (ELISAs) are widely used to quantify anti-spike receptor binding domain (RBD) immunoglobulin G (IgG) levels, providing insights into neutralizing antibody trends [22]. However, their dependence on laboratory-based microplate readers and long analysis times (up to 4 h) restricts their utility in resource-limited settings.

Microfluidic technology offers a rapid and user-friendly approach for diagnosis, yet conventional systems often rely on external liquid-driving accessories, which increase cost and limit portability [23–25]. They also

* Corresponding author.
E-mail address: zhugen.yang@cranfield.ac.uk (Z. Yang).
[1] These authors contributed equally.

https://doi.org/10.1016/j.snb.2025.138731
Received 6 May 2025; Received in revised form 29 August 2025; Accepted 7 September 2025
Available online 8 September 2025
0925-4005/© 2025 The Authors. Published by Elsevier B.V. This is an open access article under the CC BY license (http://creativecommons.org/licenses/by/4.0/).

face limitations in manufacturing and scalability, primarily due to their dependence on complex manufacturing process such as photolithography. These requirements not only increase production costs but also hinder large-scale implementation. In contrast, paper-based microfluidics presents a low-cost alternative, enabling the integration of multiple steps from sample preparation to detection on a single chip [26–28]. These devices align with the WHO-ASSURED criteria (Affordable, Sensitive, Specific, User-friendly, Robust, Rapid, Equipment-free, and Deliverable) for POCT [29,30]. By leveraging pre-designed folding sequences to control fluid directionality, paper-microfluidic devices can be engineered for simultaneous detection of viral RNA and antibodies in saliva, thereby advancing non-invasive infectious disease diagnosis.

In this study, we presented a paper-microfluidic platform for rapid and low-cost SARS-CoV-2 diagnosis that simultaneously detected viral RNA and proteins in saliva. The system integrated a streamlined saliva processing protocol incorporating collection, dilution, and lysis, a paper-based colorimetric reverse transcription loop-mediated isothermal amplification (RT-LAMP) assay for viral RNA detection using glass fiber nucleic acid extraction (LOD: 10 copies/μL), and a paper-based ELISA (p-ELISA) assay for immunoglobulin titer quantification (LOD: 0.5 ng/μL). The lyophilized reagent formulation enabled operational simplicity and long-term stability, while colorimetric signals were readable either visually or via smartphone imaging. The entire assay was completed within 60 min, providing a faster turnaround compared to kit-based methods while maintaining 93 %–106 % recovery in saliva samples. By enabling non-invasive saliva analysis and evaluation of both infection status (viral load) and immune response (antibody titers), this platform will provide comprehensive diagnostic capabilities, particularly suitable for resource-limited settings.

2. Materials and methods

2.1. Primer design and RNA synthesis

A plasmid DNA template containing a 601 bp region of the SARS-CoV-2 ORF1a gene (GenBank: NC045512.2) [31] was synthesized (Thermo Fisher Scientific, USA). The template was amplified by PCR using a forward primer encoding the T7 RNA polymerase promoter sequence (5'-TAATACGACTCACTATAGGG-3') and a gene-specific reverse primer (primer sequences are provided in Table S1). After the resulting PCR amplicons were confirmed on 2 % agarose gel, they were purified using a Zymoclean Gel DNA Recovery Kit (Zymo Research, USA). Subsequently, *in vitro* transcription (IVT) was performed using a HiScribe T7 High Yield RNA Synthesis Kit (New England Biolabs, UK). A reaction volume of 20 μL (containing 1 μg of the purified PCR products) was incubated at 37 °C for 2 h. The synthesized RNA transcripts were then purified using a Monarch Total RNA Miniprep Kit (New England Biolabs, UK). Both the PCR and LAMP primer sets targeting the ORF1a gene were designed using PrimerExplorer V5 and synthesized by Merck (Sigma-Aldrich, USA).

2.2. RT-qPCR assay and RT-LAMP assay

The concentration of synthetic SARS-CoV-2 RNA was quantified using a Qubit 4 fluorometer (ThermoFisher Scientific, USA). A stock solution of 2.4 ng/μL, equivalent to 4×10^9 copies/μL, was serially diluted to generate an RT-qPCR standard curve. RT-qPCR reactions were performed in a 20 μL volume containing 5 μL TaqMan Fast Virus 1-Step Master Mix (ThermoFisher Scientific, USA), 0.5 μL each of forward and reverse primer (20 mM), 1 μL EvaGreen dye, 5 μL probe, 3 μL RNase-free water, and 5 μL RNA template. Amplification was performed on a QuantStudio 3 Real-Time PCR system under the following conditions: initial reverse transcription at 50 °C for 2 min, followed by denaturation at 95 °C for 20 s, 40 cycles of denaturation at 95 °C for 3 s with annealing/extension at 60 °C for 30 s, and a final hold at 60 °C for 30 s. RNase-free water was included as a negative control in each run.

RT-LAMP assays were performed in both fluorescence-based and colorimetric formats. For the fluorescence assay, RT-LAMP mixture was prepared using 12.5 μL WarmStart LAMP 2 × Master Mix (New England Biolabs, UK), 0.5 μL fluorescence dye (50 ×), 2.5 μL LAMP primers (Concentrations: 2 μM F3, 2 μM B3, 16 μM FIP, 16 μM BIP, 4 μM LF, and 4 μM LB), 7.5 μL RNase-free water, and 2 μL RNA template. Reactions were incubated at 65 °C for 40 min (1 min/cycle) with fluorescence acquisition on a real-time PCR system. For the colorimetric assay, RT-LAMP mixture consisted of 10 μL WarmStart LAMP 2 × Colorimetric Master Mix (New England Biolabs, UK), 2 μL LAMP primers, 7 μL RNase-free water, and 1 μL RNA template. Reactions were incubated at 65 °C for 40 min in a heat block.

2.3. Microplate-based enzyme-linked immunosorbent assay (ELISA)

Serum levels of IgG antibodies were quantified using an indirect ELISA format. Recombinant SARS-CoV-2 Spike RBD antigen (Ag; 50 μL at 1.6 μg/mL in phosphate-buffered saline (PBS)) was immobilized by coating onto a microplate, which was subsequently incubated at 4 °C overnight. Control wells were coated with an equivalent volume of deionized water. Following incubation, the coating solution was discarded, and the wells were washed three times with 200 μL PBS containing 0.1 % TWEEN-20 (PBST). To block non-specific binding sites, 100 μL blocking buffer (10 % w/v milk concentrate in PBST) was added to each well and incubated at 37 °C for 1 h.

After another washing step (3 × 200 μL PBST), 100 μL of serially diluted primary antibody (5–80 ng/mL in PBST) was added to the wells and incubated. The plate was then washed again (3 × 200 μL PBST), and 100 μL horseradish peroxidase (HRP)-conjugated species-specific secondary antibody (diluted 1:10,000 in blocking buffer) was dispensed into each well. Following a final wash (3 × 200 μL PBST), the enzymatic reaction was initiated by adding 75 μL 3,3',5,5'-tetramethylbenzidine (TMB) substrate and incubating the plate in the dark for 15 min. The reaction was terminated by the addition of 50 μL of 1 M sulfuric acid (H_2SO_4). Absorbance was measured at 450 nm using a Varioskan LUX multimode microplate reader (Thermo Fisher Scientific, USA).

2.4. Paper-based enzyme-linked immunosorbent assay (p-ELISA)

To accommodate the limited saturation capacity of the paper substrate, a modified protocol was developed for the p-ELISA assay. The paper device was first incubated in a Petri dish containing 5 % (w/v) bovine serum albumin (BSA) for 30 min at room temperature for blocking and was stored under the same conditions until use. Following this pretreatment, 1.5 μL antigen (1.6 μg/mL in PBS) was immobilized onto each detection zone for 20 min. Unbound antigen was then removed by performing two washing steps, each using 5 μL PBST. Subsequently, 2.5 μL primary antibody, followed by 2.5 μL HRP-conjugated secondary antibody, were applied to each detection zone. The specific concentrations and dilutions for both antibodies were identical to those used in the microplate ELISA described above. Each incubation step was followed by a washing procedure with 5 μL PBST to remove unbound reagents. The device was placed on a piece of absorbent tissue to prevent direct contact with the bench surface and to facilitate capillary action. Finally, colour development was initiated by adding 2.5 μL TMB-H_2O_2 substrate solution to each detection zone.

2.5. Saliva treatment

Artificial saliva for pharmaceutical research was purchased from Merck (Sigma-Aldrich, USA). To mimic saliva samples, 10 μL SARS-CoV-2 ORF1a fragment (4×10^4 copies/μL) was spiked into 90 μL saliva. Before measuring with relevant assays, samples were pretreated based on HUDSON (heating unextracted diagnostic samples to obliterate nucleases) [32] as well as an adapted and optimized protocol [33] . A ratio

of 8 μL Tris-EDTA (pH 8.0), 0.1 μL Rnase inhibitor and 1.9 μL protease K were mixed to make a dilution buffer for saliva samples. The thermal protocol used was as follows: initial incubation at room temperature (20–25 °C) for 10 min, followed by a transition to 65 °C for 10 min, and finally incubation at 100 °C for 12 min. Alternatively, an RNA purification step was performed with an RNeasy Kit (Qiagen, Germany). A follow-up RT-qPCR assay was performed to ensure the efficiency of saliva treatment.

2.6. Data analysis

Result images were captured by iPhone 12 and analysed by Fuji/Image J (National Institutes of Health, USA), and colour quantification was evaluated using the formula presented Eqs. (1) and (2). Each detection zone was cropped within a 17 × 17 circle (Image J scale) and divided into Red (R), Green (G), and Blue (B) channels to measure the mean grey values. A control (absence of HRP signal) was used as a reference to estimate the background signal noise, which was subtracted from the measurements. Herein, the mean grey value was calculated for each detection zone as in Eq. (1) and Eq. (2):

$$\Delta RGB = \sqrt{(R - R_0)^2 + (G - G_0)^2 + (B - B_0)^2} \quad (1)$$

$$RGB = \Delta RGB_S - \Delta RGB_C \quad (2)$$

Where *R, G,* and *B* are the mean grey values captured for samples on the detection zone, while R_0, G_0, and B_0 are the mean grey values captured on the control zone. Furthermore, the negative control (absence of primary antibody) signal (ΔRGB_C) is calculated and subtracted from ΔRGB_S to obtain the final RGB intensity. ΔRGB_S stands for the signal produced by samples, while an ΔRGB_C is the signal generated by the control.

3. Results and discussion

3.1. Fabrication and optimization of paper-microfluidic devices

SARS-CoV-2 infection presents a specific diagnostic temporal window, wherein viral RNA is detectable by RT-qPCR assay within 24–48 h post-infection, but neutralizing antibodies produced by the adaptive immune response do not appear until 5–7 days later (Fig. 1a). Inspired by this challenge, we presented a paper-based microfluidic platform for rapid and low-cost SARS-CoV-2 diagnosis. This platform detected both

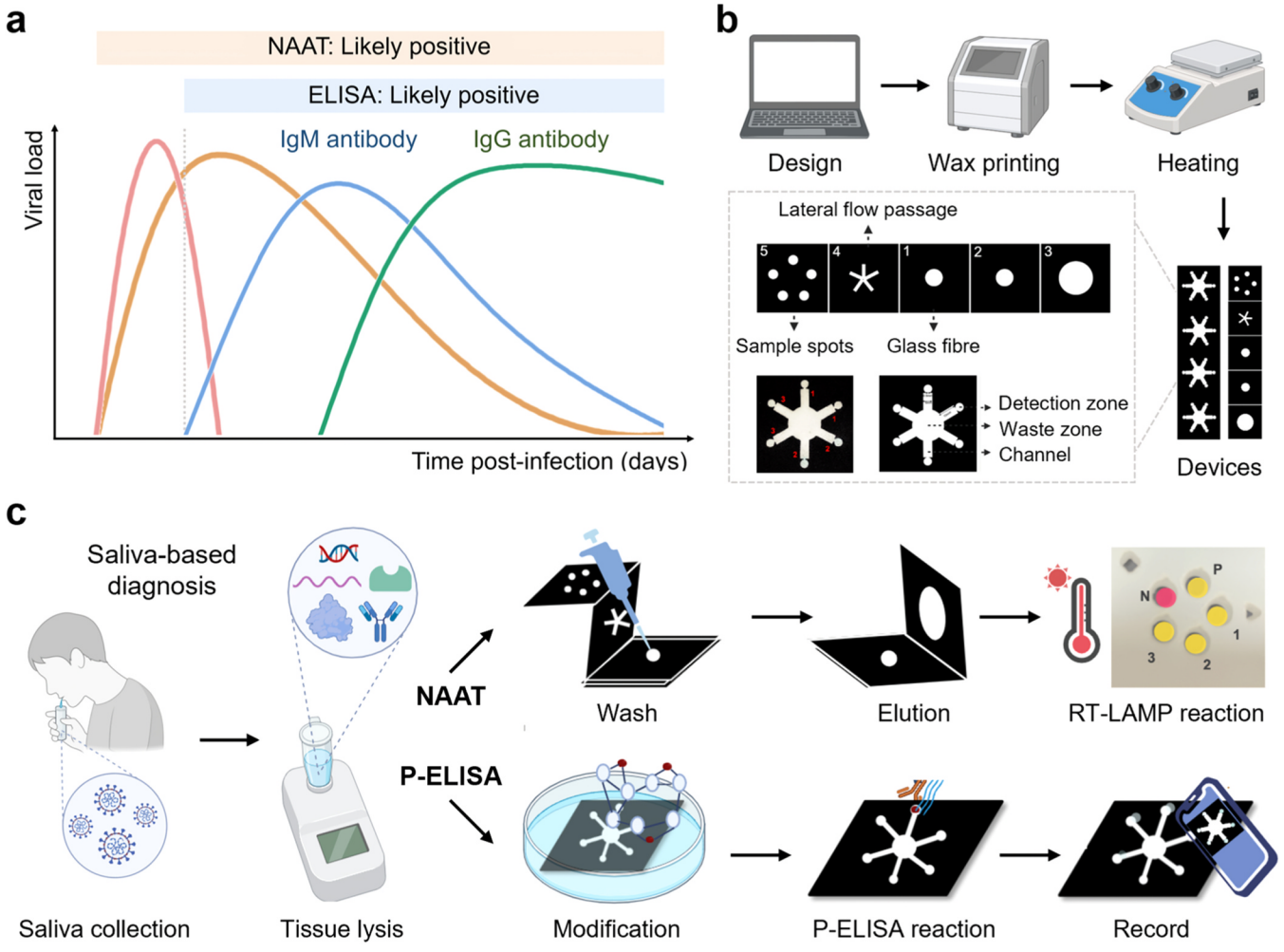

Fig. 1. Paper-microfluidic platform for SARS-CoV-2 diagnosis. (a) Diagnostic temporal window. SARS-CoV-2 exhibits viral RNA detectable by RT-qPCR assay within 24–48 h post-infection. In contrast, neutralizing antibodies emerge only after 5–7 days via adaptive immune response. (b) Device architecture and fabrication, including design, wax-printing, baking, and assembly. NAAT module comprised a glass fiber disk, lateral flow channels, and reaction chambers. p-ELISA module comprised 6 radial detection zones around a central waste reservoir. (c) Operational workflow. Collected saliva underwent dilution and lysis (65 °C, 10 min; 100 °C, 12 min). NAAT detection involved sample application to glass fiber, wash buffer purification, origami folding, elution buffer transfer, and RT-LAMP assay at 65 °C (40 min). p-ELISA detection involved surface blocking (5 % BSA), RBD antigen immobilization, sequential loading of IgG and HRP-conjugated secondary antibody, colorimetric development (TMB/H_2O_2), smartphone imaging and quantitative analysis (ImageJ).

viral RNA and antibodies in a single saliva sample, offering a comprehensive solution across the critical early phase of infection.

The foundational design of the paper-microfluidic device for RT-LAMP assay was adapted from the work of Yang et al. [34]. The modified paper device comprised five distinct components, each patterned with hydrophilic (white) and hydrophobic (black) regions. Rectangular hydrophilic channels (4 mm × 2 mm) were incorporated for controlled fluid transport, paired with a circular waste absorption zone (25 mm diameter). Fabrication was achieved via wax printing on Whatman chromatography paper, followed by heating at 120 °C for 1 min on an isothermal hotplate to melt the wax and define fluidic channels (Fig. 1b). The design incorporated a filter paper with wax-defined hydrophobic barriers, a single sided adhesive acetate film-sealed plastic plate housing five paper spots (3 mm diameter) as LAMP reaction chambers, and a glass fiber disk (6 mm diameter) for nucleic acid absorption.

In our optimized design, key modifications were implemented to improve performance. Paper spots were reduced from 4 mm to 3 mm diameter to minimize sample volume requirements while preserving detection sensitivity. Glass fiber disk was enlarged from 4 mm to 6 mm diameter to enhance nucleic acid adsorption capacity and reduce elution losses. Channels were narrowed from 6 mm × 3 mm to 4 mm × 2 mm to shorten the elution path, thereby minimizing nonspecific nucleic acid adsorption and improving delivery efficiency to reaction chambers. Waste absorption zone was expanded from 15 mm to 25 mm diameter to increase waste capacity, reducing contamination risks and operational complexity. These modifications reduced critical limitations of the original design, improving nucleic acid recovery and operational robustness, without compromising analytical performance.

Saliva presents a complex biological matrix containing inhibitors known to compromise the efficacy of NAATs and immunoassays [35]. Key inhibitors relevant to this study include: mucins that bind RNA and hinder primer accessibility [36]; nucleases that degrade RNA and reduce sensitivity [37]; proteases capable of cleaving antibody conjugates in p-ELISA assay [38]; and polysaccharides that chelate Mg^{2+}, a critical cofactor for RT-LAMP reactions [39]. Furthermore, human genomic DNA can compete with viral targets for binding sites on glass fibers. Additional small molecules may interfere with nucleic acid hybridization, while other contaminants contribute to nonspecific adsorption. These inhibitors can diminish analytical performance by inhibiting enzymatic activity or promoting nonspecific amplification.

Considering the above interfering factors, Fig. 1c outlines the streamlined sample processing workflow including saliva collection and tissue lysis. The thermal protocol comprised an initial 10-min incubation at room temperature (20–25 °C), followed by a 10-min heating phase at 65 °C, and a final 12-min denaturation step at 100 °C. To mitigate the interference, saliva samples were subjected to dilution, reducing inhibitor concentrations below an interference threshold. The dilution buffer, consisting of 8 μL Tris-EDTA, 0.1 μL RNase inhibitor, and 1.9 μL proteinase K, was homogenously mixed to ensure complete sample lysis. This formulation effectively disrupted mucin networks while concurrently preserving RNA integrity.

For the NAAT device, a glass fiber disc was positioned at the center of panel 1 to serve as the sample application zone. A corresponding hole was punctured in panel 2 to facilitate the introduction of wash and elution buffers. A custom-fabricated plastic plate was used to form a sealed reaction chamber. The assay started with folding and clamping panels 2 and 3. The processed saliva sample was applied to the glass fiber disc, followed by the addition of wash buffer (70 % ethanol). Subsequently, panels 4 and 5 were folded to align panel 1 with panel 2. Elution buffer (ddH_2O) was introduced to elute the nucleic acids from glass fiber. Finally, the eluted sample spots were affixed to the chambers to initiate RT-LAMP reaction. This approach ensured a reproducible and efficient workflow for downstream nucleic acid amplification.

Previous research has explored various designs to adapt ELISA for paper-based platforms. For instance, Kasetsirikul et al. demonstrated the detection of SARS-CoV-2 antibodies on a paper device employing a double-sided lamination to contain the entire process within a single zone [40]. Although such mainstream developments may not represent the optimal configuration, they inspired for our design. A principal challenge in paper-based immunoassays is reducing non-specific binding. A novel design utilizing Whatman chromatography paper was presented in Fig. 1c, with parameters provided in Fig. S1 and Table S2. A central detection zone was connected via radial channels to a peripheral waste zone.

Comparative fluid dynamics analysis revealed that a larger detection zone diameter (Design 1) increased the time required for sample dispersion to the periphery. This design delayed sample entry into the channels and resulted in longer processing times, even with the same channel length. In contrast, designs with identical and smaller detection zone diameters (Designs 2 and 3) exhibited simultaneous sample arrival at the periphery. However, the increased channel length in Design 2 increased fluid transport time to the waste zone. Design 3, with a 5 mm detection zone diameter and a 10 mm channel length, was selected for p-ELISA assay due to its minimal overall fluid transport time. The final design consisted of a central waste zone (25 mm diameter) connected to six smaller detection zones via 5 mm channels.

On the other hand, the p-ELISA device was first incubated in 5 % BSA for 30 min to block non-specific binding sites and subsequently stored at room temperature. Following this blocking step, 1.5 μL antigen was immobilized onto each detection zone for 20 min. Unbound antigen was then removed via two sequential 5 μL washes with PBST. Subsequently, 2.5 μL primary antibody and 2.5 μL secondary antibody were sequentially loaded onto their respective zones, with each immunoreaction step followed by a PBST wash to remove unbound reagents. Finally, 2.5 μL TMB-H_2O_2 substrate solution was added to each detection zone to facilitate colorimetric development. The resulting blue colour intensity was captured using a smartphone camera and quantified using Fuji/Image J software.

3.2. Sensitivity of fluorescent RT-LAMP assay

The RT-LAMP assay was designed to target a specific region of ORF1a gene (GenBank: MN908947), with the primer binding locations detailed in Fig. 2a. A schematic illustrating the molecular mechanism of LAMP reaction was presented in Fig. 2b. The target sequence was detected by both RT-qPCR and RT-LAMP assays, confirming the efficiency of IVT reaction (Fig. S2). Furthermore, agarose gel electrophoresis analysis confirmed the absence of non-specific amplification, thereby demonstrating the high specificity of RT-qPCR assay.

To validate the compatibility of RT-LAMP assay with paper-microfluidic device, RNA samples were first analyzed on a thermocycler to establish analytical sensitivity. Serial dilutions of RNA (4–4 $\times 10^3$ copies/μL) were tested using a FAM-based fluorescence readout (Fig. 3a). Robust amplification was detected down to 40 copies/μL, equivalent to 80 copies per 25 μL reaction volume (3.2 copies/μL). The feasibility for complex biological matrices was further assessed using spiked saliva samples. For absolute quantification, a standard curve was generated by RT-qPCR assay for the calculation of recovery rates. No amplification was observed in untreated saliva samples, highlighting the necessity for a sample pretreatment protocol to remove inhibitors. The standard curve exhibited a strong linear relationship (Fig. 3d). The calculated recovery rates for pretreated saliva samples fell within an acceptable range of 80–120 % [41], confirming the efficacy of our sample treatment process.

3.3. Colorimetric RT-LAMP assay on paper-microfluidic device

Fluorescent RT-LAMP assay was adapted for colorimetric RT-LAMP assay on a paper-microfluidic device to facilitate simple colorimetric readout visible to the naked eye. All device components were subjected to UV decontamination for 30 min to maintain sterility. The workflow

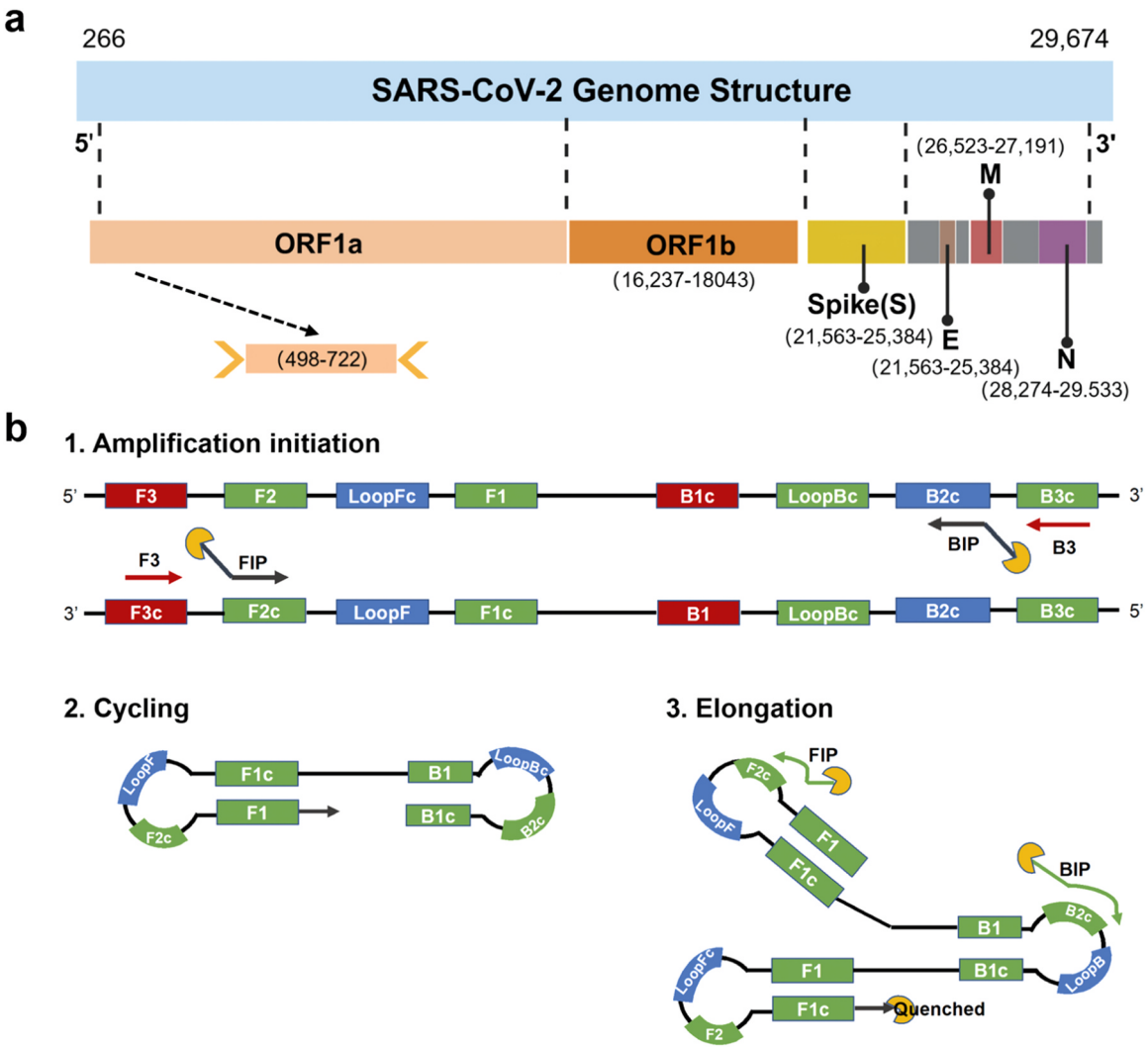

Fig. 2. SARS-CoV-2 genome and molecular mechanism of LAMP assay. (a) Genomic organization of SARS-CoV-2, indicating the location of ORF1a gene. The position and length of RT-LAMP amplicons are denoted by a dashed arrow. (b) Schematic illustrating the molecular mechanism of LAMP reaction. The process involved auto-cycling strand displacement DNA synthesis to achieve amplification of the target sequence. The final products consisted of a mixture of stem-loop DNA structures and targeted inverted repeats, forming a cauliflower-like structure with multiple loops.

involved applying the pre-treated saliva sample to the sample inlet, where it migrated through the microfluidic channels via capillary action to elute nucleic acids. The reaction mixture was introduced to initiate RT-LAMP reaction within the sealed device. Initial validation was performed using higher concentration spiked saliva samples, achieving an LOD of 200 copies/μL (Fig. S3). Colorimetric analysis revealed no significant difference in the colour ratios among positive samples. A statistically significant difference was observed only between these samples and a negative control. The detection zone exhibited a definitive color transition from red to yellow within 35 min. ImageJ was employed to quantitatively assess the correlation between the observed colour shift and viral load.

The tolerance of RT-LAMP assay to inhibitors in complex matrices allowed for the omission of purification when testing mimic saliva samples. However, salivary constituents could still potently inhibit RT-LAMP amplification. Using a colorimetric readout, the assay successfully detected SARS-CoV-2 RNA across a range of 12–276 copies/μL, yielding an LOD of 28 copies/μL (Fig. 4a). A visible color change from red to yellow was observed in all positive samples, including the lowest concentration, while the negative control remained unchanged. This transition was attributed to the gradual acidification of the reaction environment caused by proton accumulation during RT-LAMP amplification [42]. The optimized colorimetric protocol enabled rapid detection, with results achievable within 35 min.

A critical finding was that a pretreatment method comprising proteinase K and RNase inhibitor (in Tris-EDTA, pH 8.0) significantly enhanced RT-LAMP sensitivity in saliva, even without RNA purification. When this pretreatment was applied prior to RT-LAMP assay in tubes, the LOD was significantly improved to 28 copies/μL. Although the sensitivity of the device was lower than that of laboratory-based equipment, its LOD remained clinically relevant for rapid diagnosis, as the viral loads in most infected individuals far exceeded 200 copies/μL. A comparable colorimetric saliva assay also reported an LOD of 200 copies/μL [43]. However, that platform employed a lateral flow test (LFT) format, which was limited to single-plex analysis and suffered from a longer 60-min incubation time. Successful validation with clinical samples would establish this device as a rapid and less invasive testing tool.

To explore the potential for semi-quantitative analysis, a reference colour bar was established based on the hues observed at various target concentrations and time intervals (Fig. 4b). While the current device provided a semi-quantitative result, we propose that future iterations could be engineered for quantitative measurement, potentially through integration with smartphone-based colorimetry systems as reported

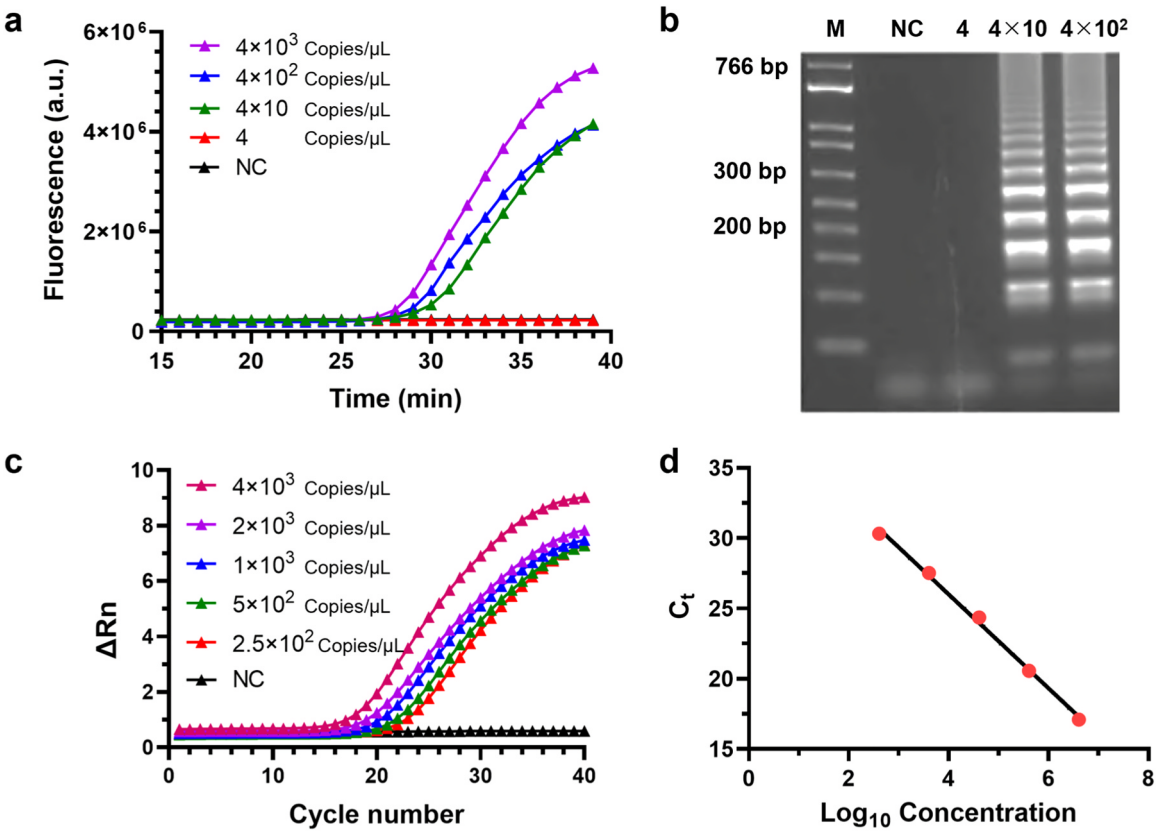

Fig. 3. Sensitivity of fluorescent RT-LAMP assay and RT-qPCR assay. (a) Amplification curves of RT-LAMP assay targeting ORF1a gene. (b) Agarose gel electrophoresis analysis of RT-LAMP products. M, DNA molecular weight marker; NC, negative control. (c) Amplification curves of RT-qPCR assay targeting ORF1a gene in spiked saliva samples. (d) RT-qPCR standard curve for absolute quantification. The linear regression equation is $Y = -3.34X + 39.37$ ($R^2 = 0.99$). Data are presented as mean ± standard deviation (SD) (n = 3).

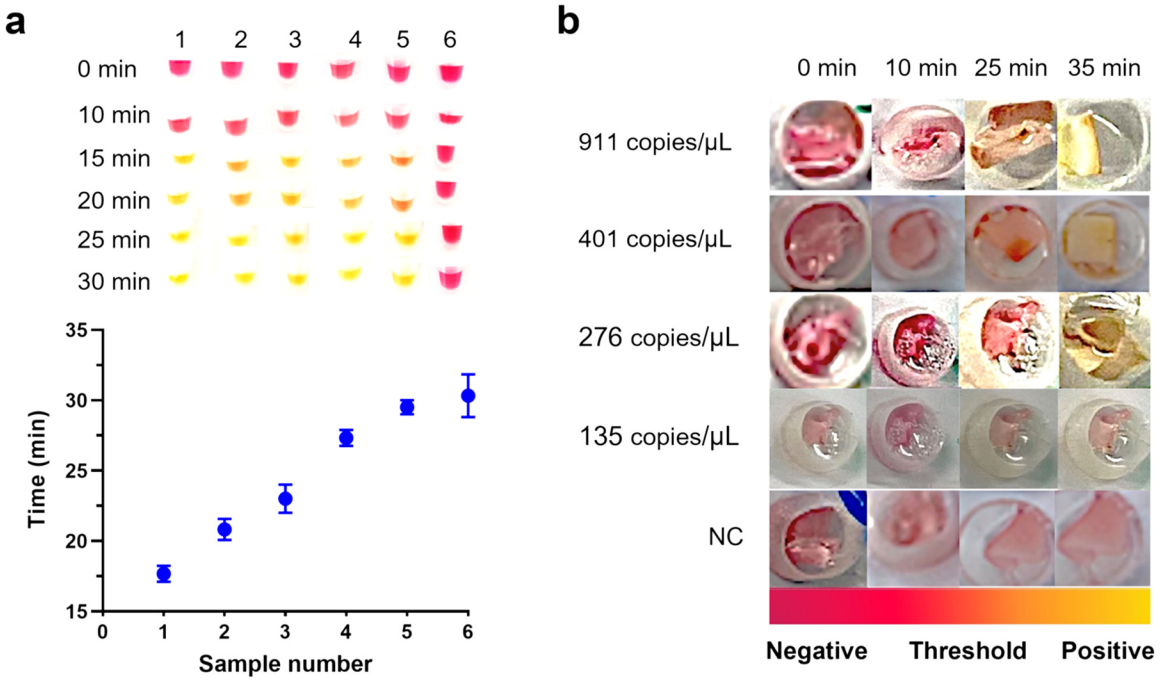

Fig. 4. Sensitivity of colorimetric RT-LAMP assay in mimic saliva samples. (a) Tube-based colorimetric RT-LAMP assay. Top panel: Colorimetric results for various target concentrations at distinct reaction time points. Reactions were terminated by ice immersion, and images were captured using an iPhone 12. Bottom panel: Timeline of the color transition (red to yellow) for each concentration. Concentrations (1–6): 276 copies/μL, 135 copies/μL, 64 copies/μL, 28 copies/μL, 12 copies/μL. Data are presented as mean ± standard deviation (SD) (n = 3). (b) Paper-based colorimetric RT-LAMP assay. Images showed colorimetric responses across various target concentrations and time intervals. The bottom scale defined the range for positive (yellow) and negative (red) results. NC, negative control.

elsewhere [44]. The development of a mobile application could enable rapid and portable data interpretation. To minimize false positives from amplicon carryover, dUTP and thermolabile uracil-DNA glycosylase (UDG) were incorporated into the reaction mixture [45]. UDG enzyme remained active at lower temperatures (25–37 °C), cleaving uracil bases in any dU-containing amplicons and rendering them unamplifiable. UDG enzyme was later inactivated at 60–65 °C, allowing the WarmStart DNA polymerase to amplify the target nucleic acids with uncompromised efficiency.

3.4. In-house indirect ELISA assay on microplate

To establish a quantitative serological assay, an indirect ELISA protocol was developed for the detection of anti-SARS-CoV-2 IgG (Fig. S4). Microplate-based format was selected to enable the precise determination of optimal conditions, which could be translated to a paper-microfluidic device. Optimization parameters consisted of immobilized antigen concentration, serum dilution factors, and blocking buffer composition. In Fig. S5, optimal conditions were determined to be an antigen concentration of 1.6 μg/mL and the use of 10 % (w/v) milk concentrate as an effective blocking agent. A standard curve relating absorbance to IgG concentration demonstrated a linear relationship, defined by the equation $Y = 0.0126X + 0.0188$ ($R^2 = 0.989$) (Fig. 5a). The calculated LOD (5 ng/mL) represented an improvement in sensitivity over previous studies (LOD: 3.6 μg/mL) [46,47].

To evaluate the feasibility of using saliva as a diagnostic matrix, its potential inhibitory effects were assessed. An initial recovery study revealed that untreated saliva significantly interfered with specific antibody-antigen binding. In Fig. 5b, the recovery rates for spiked saliva samples were outliers beyond the acceptable 80–120 % range [48], with at least two concentrations exceeding the upper limit of quantification (ULOQ), indicating substantial matrix interference. To overcome this limitation, a simple pretreatment protocol was implemented, involving a 1:1 dilution of saliva in buffer followed by centrifugation at 15, 000 × g and 4 °C for 20 min. This treatment effectively mitigated the matrix effect, as confirmed by a sigmoidal four-parameter logistic (4PL) curve fit and supported by quantitative RGB analysis (Figs. 5c, 5d). This improvement established pretreated saliva as a viable matrix for accurate detection.

To evaluate assay specificity, p-ELISA assay was challenged with the antibodies against common respiratory viruses. They are considered to cause cross-reactive symptoms or share structural homology with SARS-CoV-2, including influenza A and B, Middle East respiratory syndrome coronavirus (MERS-CoV), severe acute respiratory syndrome coronavirus (SARS-CoV), and four endemic human coronaviruses (HCoV-OC43, HCoV-229E, HCoV-NL63, and HCoV-HKU1). The assay exhibited high specificity for SARS-CoV-2, as demonstrated by the negligible absorbance in the presence of non-target antibodies (Fig. S6). A known cross-reactivity was observed with SARS-CoV IgG, due to shared epitopes within the conserved nucleocapsid protein [49]. The critical need for such a specific test was highlighted by the symptomatic overlap between SARS-CoV-2 infection and common colds caused by other coronaviruses

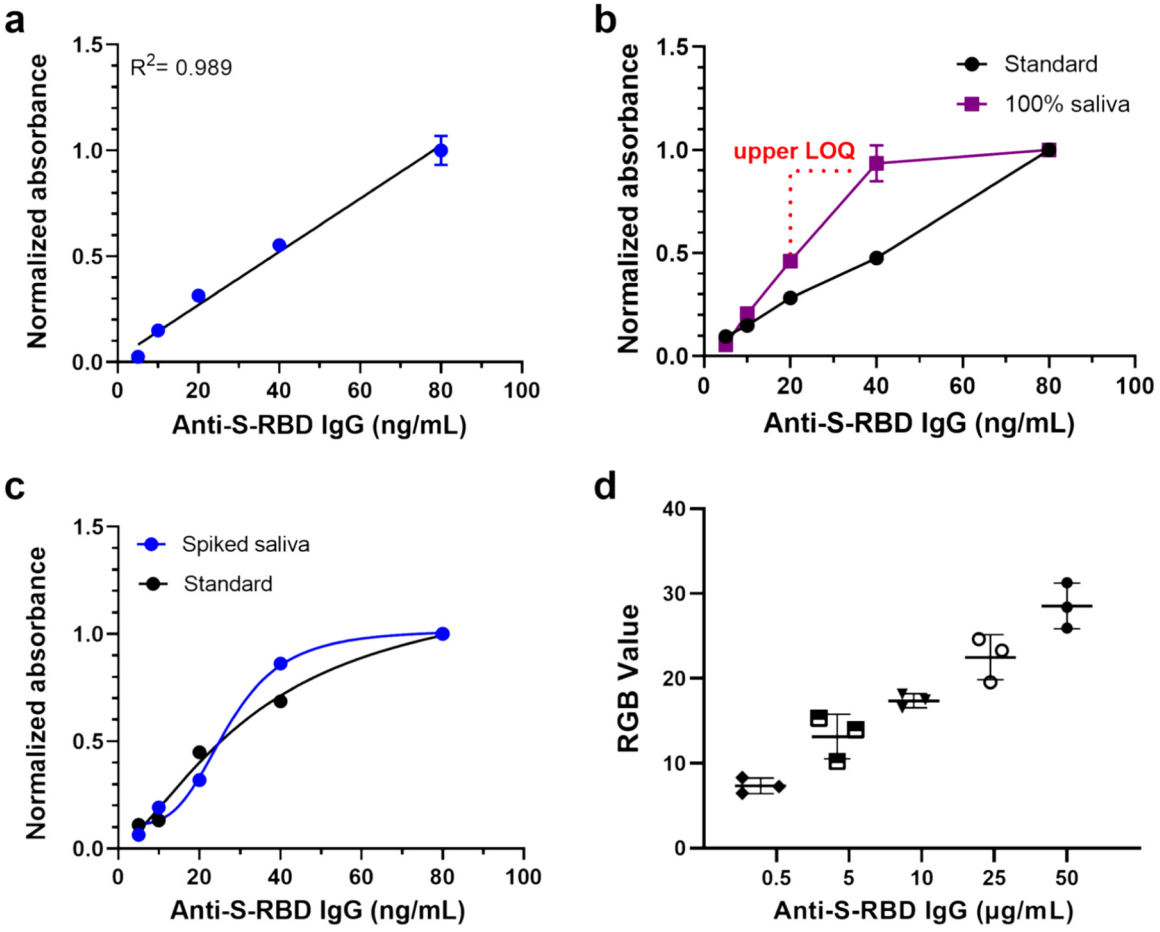

Fig. 5. Sensitivity of indirect ELISA assay in mimic saliva samples. (a) Standard curve for the indirect ELISA assay. The linear regression was defined by the equation $Y = 0.0126X + 0.0188$ ($R^2 = 0.989$). (b) Assessment of saliva matrix effects. The reduced linearity and abnormal curve in saliva indicated substantial interference with antibody-antigen binding ($R^2 < 0.8$). (c) Validation of matrix interference mitigation. A 4PL curve fit demonstrated excellent recovery for the recombinant antibody in pretreated saliva ($R^2 = 0.99$). (d) Quantification of colorimetric readouts. RGB analysis demonstrated a correlation between colour intensity and analyte concentration. Data are presented as mean ± standard deviation (SD) (n = 3).

(e.g., cough, fever, and headache), which could lead to misdiagnosis based on symptoms alone [50]. Our p-ELISA assay provided a rapid and reliable approach to distinguish SARS-CoV-2 from other prevalent respiratory pathogens.

3.5. Viral RNA and antibody detection on paper-microfluidic platform

Although the optimized ELISA assay demonstrated high sensitivity, it was imperative to align its dynamic range with the physiologically relevant concentrations of antibodies in clinical samples. Based on the serological profiles of vaccinated, convalescent, and seronegative individuals, IgG concentrations in biological fluids can vary significantly. Reported levels range from 0.6–3.3 μg/mL in convalescent unvaccinated individuals, rising to a mean of ~88 μg/mL post-vaccination [47]. In contrast, seronegative individuals typically maintain a baseline IgG level of ~0.2 μg/mL, irrespective of vaccination status. To ensure the clinical relevance of our assay, the working concentration range was therefore calibrated to 0.5–50 μg/mL.

Initial experiments in a microplate format indicated that a 1:1 dilution of saliva in buffer was sufficient to reduce matrix effects. However, this dilution rate proved insufficient when transferred to a paper-microfluidic device (Fig. S5). The salivary matrix continued to hinder antigen-antibody binding, likely due to increased viscosity and nonspecific interactions within the porous fiber network. Quantitative RGB analysis of the colorimetric output was employed to assess the performance of different dilution ratios (Fig. 6a). The 1:4 dilution yielded a non-proportional signal response, particularly at lower antibody concentrations, confirming its inadequacy for reliable quantification. In contrast, a 1:10 dilution ratio produced a robust and proportional dose-response relationship across a clinically relevant concentration range of 0.5–50 μg/mL (Fig. 6b). Higher dilution ratios (1:20, 1:40, and 1:50) maintained this consistent trend but offered no significant analytical changes.

These findings were supported by the previous studies. ELISA protocols for human serum usually employ 1:10 or 1:100 dilutions to suppress background interference [51]. Furthermore, our approach was consistent with precedents for salivary immunoassays (1:10 dilution), including SARS-CoV-2 Spike IgA detection [52] and autoantibody diagnosis of autoimmune diseases [53]. Based on consistency for cost-effectiveness, workflow simplicity, and optimal analytical performance, the 1:10 dilution ratio was selected for p-ELISA assay. The optimized p-ELISA assay exhibited excellent linearity, defined by the equation $Y = 0.41X + 11.07$ ($R^2 = 0.97$) (Fig. 6c). The calculated LOD was below 1 ng/μL, with a visually confirmable LOD of 0.5 ng/μL. This

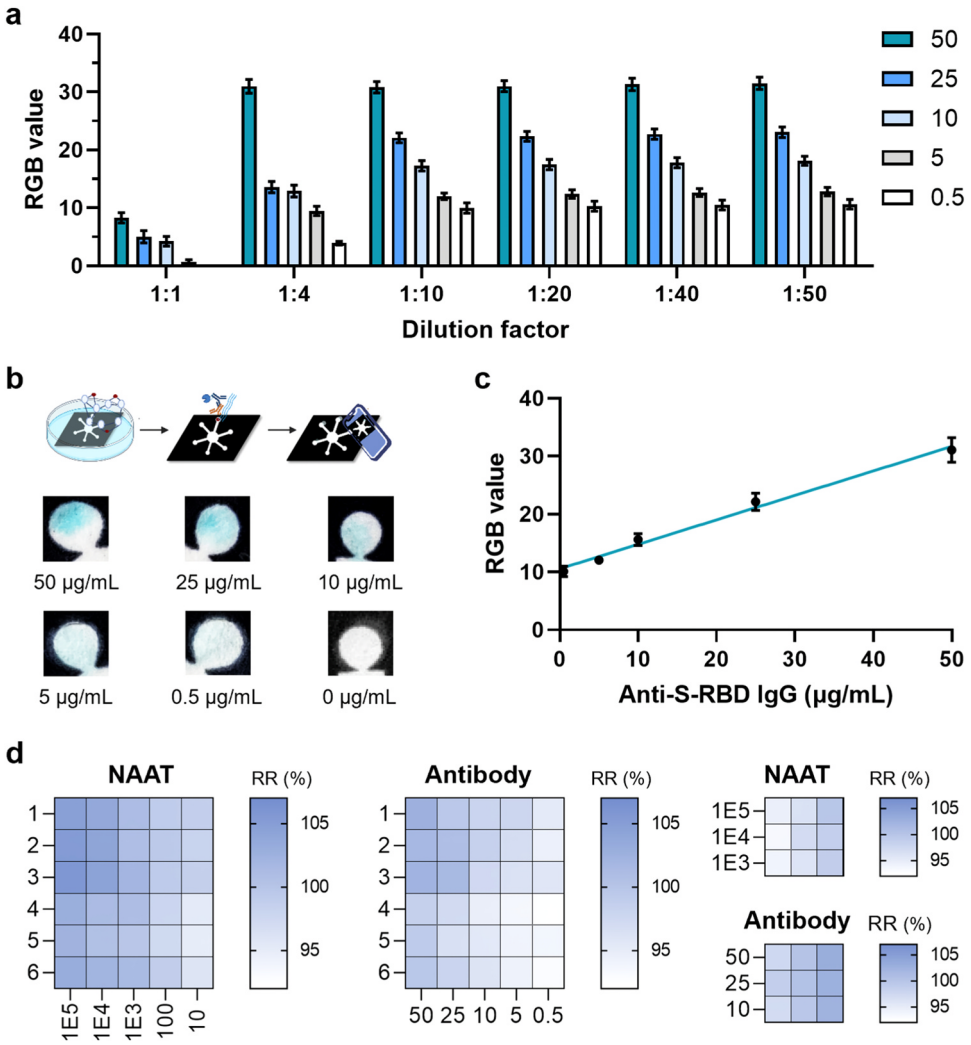

Fig. 6. Paper-microfluidic platform for saliva diagnosis. (a) RGB colorimetric analysis of SARS-CoV-2 IgG in saliva across six dilution ratios (1:1–1:50). (b) Representative p-ELISA assay images for IgG detection at 1:10 dilution, tested at concentrations ranging from 0 to 50 μg/mL. (c) Linear regression of RGB intensity versus IgG concentration (1:10 dilution; n = 3; error bars: mean ± SD). (d) Comparative recovery analysis. Left panel: Heatmap of RNA recovery rates (10–10^6 copies/μL) via paper-based RT-LAMP assay. Middle panel: Heatmap of IgG recovery (0.5–50 μg/mL) via p-ELISA assay. Right panel: Heatmap evaluating concurrent RNA/antibody recovery in spiked saliva. 1–3, spiked artificial saliva; 4–6, spiked clinical saliva; RR, recovery rate.

sensitivity was superior to that of many commercial serum-based ELISA kits (LOD: 10 ng/μL) [54] and was sufficiently low to distinguish between immune and non-immune individuals based on salivary antibody titers.

Compared with a colorimetric paper-based method for the detection of SARS-CoV-2 antibodies (Dynamic range: 1.0–50 ng/μL; LOD: 9 ng/μL) [40], we presented a wider linear dynamic range of 0.5–60 ng/μL with a lower LOD of 0.5 ng/μL. However, antibody assays cannot achieve detection rates comparable to those of NAATs in the early infection stages, as humoral responses require a time lag for development after viral antigen stimulation. The immune response is individualized, as the antibodies produced by the immune system only reach detectable levels between 5 days and 2 weeks post-infection. ELISA assay alone was only employed for confirming active cases of infection or identifying SARS-CoV-2 immune cases. Therefore, we proposed combining paper-based NAATs with p-ELISA assay to address the inadequacy of serological immune-testing for early diagnosis.

To assess the accuracy of our paper-based microfluidic platform for concurrent viral RNA and antibody detection, spike-and-recovery experiments were performed using both artificial and clinical saliva (Fig. 6d). For RNA quantification, the paper-based RT-LAMP assay demonstrated recovery rates of 98.12–105.73 % in artificial saliva and 94.89–103.06 % in clinical saliva. Parallel evaluation of IgG via p-ELISA assay yielded recoveries of 94.36–102.45 % (artificial saliva) and 92.48–99.67 % (clinical saliva). In addition, SARS-CoV-2 RNA and IgG were spiked into the same clinical saliva samples to evaluate cross-interference during co-detection. IgG recovery remained robust (97.07–102.95 %) in the presence of RNA, while RNA recovery was minimally affected (93.31–99.82 %) despite antibody coexistence. These findings demonstrated the platform's robust accuracy and reliability in complex salivary matrices, while maintaining multiplexed detection capability without cross-interference.

The reproducibility of our paper-based RT-LAMP assay and p-ELISA assay was evaluated using intra- and inter-assay coefficients of variation (CV). Intra-assay CV was defined as the variability among replicate measurements performed on the same sample within a single paper disc [55]. Inter-assay CV was defined as the variability among measurements performed on the same sample using different paper discs. RNA standards at low (10 copies/μL), medium (10^3 copies/μL), and high (10^6 copies/μL) concentrations were used as analytes. Intra-assay CV values ranged from 3.5 % to 4.6 %, while inter-assay CV values ranged from 4.1 % to 5.8 %. Antibody standards at low (5 ng/μL), medium (25 ng/μL), and high (50 ng/μL) concentrations were used as analytes. Intra-assay CV values ranged from 4.3 % to 6.5 %, while inter-assay CV values ranged from 5.6 % to 7.4 %. These findings indicated that both paper-based RT-LAMP assay and p-ELISA assay exhibited high reproducibility.

The long-term stability of paper-microfluidic devices was investigated at 4 °C and room temperature over one month. 10 % (w/v) trehalose (a non-reducing disaccharide known for its protein-stabilizing properties) and silica gel bead desiccants were incorporated during storage to improve analytical performance. For the paper-based RT-LAMP assay, devices stored at 4 °C exhibited superior stability compared to those stored at room temperature (Fig. S7). Although stability declined within the first 1–2 weeks, activity was preserved after one month at both storage conditions. After 10 days, 93 % and 89 % of stability were retained at 4 °C and room temperature, respectively. Similarly, for the p-ELISA assay, devices stored at 4 °C demonstrated greater stability than those stored at room temperature. After 10 days, 83 % and 76 % of stability were maintained at 4 °C and room temperature, respectively.

Our results were consistent with prior studies, illustrating the storage stabilizing effect of trehalose. For instance, in a paper-based colorimetric assay, enzyme activity improved from 3 % to 10 % with trehalose. Similarly, the half-life of paper-based glucose assay reagents increased from 11 days to 40–50 days with trehalose [56]. The signal degradation during storage may result from protein denaturation during drying, where evaporating water molecules disrupted the tertiary and quaternary structures. This phenomenon agreed with the findings of a 90 % signal reduction after enzyme storage in paper-based assays [57]. Therefore, our paper-based microfluidic platform exhibited acceptable stability, making them suitable for long-term storage and transportation, particularly in resource-limited settings.

The paper-based microfluidic platform could effectively address salivary inhibitor challenges through sample pretreatment, optimized architecture, and strategic buffer. Consistent detection limits were demonstrated for RNA detection (10 copies/μL) and IgG quantification (0.5 ng/μL) in both saliva and buffer controls, which matched or exceeded sensitivity of conventional RT-qPCR and ELISA assay. Our platform also reduced the cost of nucleic acid and antibody detection by 70–80 % compared to standard laboratory-based methods (Table S3). The dynamic range covered clinically relevant concentrations for RNA (10–10^6 copies/μL) and IgG (0.5–50 ng/μL). Comparison with reported methods (Table S4) revealed that our platform achieved comparable or superior performance. For instance, a dual RT-LAMP assay achieved an LOD of 100 copies/μL for SARS-CoV-2 RNA in saliva [58], while an immunoassay employing variable fragments detected antigens with an LOD of 3 pmol per assay [59]. Furthermore, a nanosensor utilizing aluminum oxide reported an LOD of 1 ng/μL for IgG antibodies [60].

Despite the platform's many advantages, it may suffer from some limitations of the wax-printed paper substrate. The material properties of paper, such as its porosity and fiber structure, are different from those of PCR tubes or 96-well microplates. These differences can lead to non-uniform fluid distribution following capillary-driven flow, which in turn introduces variability into the colorimetric readout and complicates RGB analysis. Future research should focus on several advancements, including integration of pre-filtration modules to concentrate analytes and remove inhibitors, investigation into the interactions between filter paper fibers and protein structure, and exploration of advanced materials and surface modification techniques (e.g., functional coatings and cross-linking agents) to improve device robustness.

4. Conclusion

In summary, our study validated a standardized saliva treatment protocol that rendered this biofluid amenable to analysis on a paper-microfluidic platform. We demonstrated the feasibility of employing low-cost, rapid, and multiplexed paper-microfluidic devices to perform RT-LAMP and ELISA assays for the detection of SARS-CoV-2 RNA and antibodies in saliva. The sensitivity was comparable to standard RT-qPCR and commercial ELISA kits, while the entire assay time was reduced from 5 h to 1 h. These findings highlighted the significance of adopting POCT strategies that combined NAATs with immunoassays to improve diagnostic accuracy. Simultaneous analysis can facilitate determination of the stage of infection and potential patient infectivity, providing valuable information for classification and treatment. This paper-microfluidic platform holds great potential for development into a user-friendly diagnostic kit capable of comprehensively analyzing infection and immune status, thereby strengthening future public health management strategies.

CRediT authorship contribution statement

Yuwei Pan: Writing – original draft, Validation, Methodology, Investigation. **Xuanye Ma:** Writing – original draft, Validation, Methodology, Investigation. **Iva Chianella:** Writing – review & editing, Validation, Investigation. **Zhugen Yang:** Writing – review & editing, Supervision, Resources, Conceptualization.

Declaration of Competing Interest

The authors declare that they have no known competing financial

interests or personal relationships that could have appeared to influence the work reported in this paper.

Acknowledgements

This project was supported by UK Research and Innovation Natural Environment Research Council Fellowship grant (NE/R013349/2), National Wastewater Epidemiology Surveillance Programme (NE/V010441/1), and Leverhulme Trust Research Leadership Awards (RL-2022–041).

Appendix A. Supporting information

Supplementary data associated with this article can be found in the online version at doi:10.1016/j.snb.2025.138731.

Data availability

Data will be made available on request.

References

[1] M.U.G. Kraemer, et al., Artificial intelligence for modelling infectious disease epidemics, Nature 638 (2025) 623–635.
[2] G. Li, et al., Therapeutic strategies for COVID-19: progress and lessons learned, Nat. Rev. Drug Discov. 22 (2023) 449–475.
[3] E.J. Chow, T.M. Uyeki, H.Y. Chu, The effects of the COVID-19 pandemic on community respiratory virus activity, Nat. Rev. Microbiol 21 (2023) 195–210.
[4] B.A. Betthäuser, A.M. Bach-Mortensen, P. Engzell, A systematic review and meta-analysis of the evidence on learning during the COVID-19 pandemic, Nat. Hum. Behav. 7 (2023) 375–385.
[5] J. Budd, et al., Lateral flow test engineering and lessons learned from COVID-19, Nat. Rev. Bioeng. 1 (2023) 13–31.
[6] R.G. Mannino, et al., The critical role of engineering in the rapid development of COVID-19 diagnostics: lessons from the RADx tech test verification core, Sci. Adv. 9 (2023) eade4962.
[7] X. Lu, et al., From crisis to innovation in point-of-care testing: lessons from the COVID-19 pandemic and future directions, Trends Anal. Chem. 184 (2025) 118131.
[8] C.S. Laxton, et al., The potential of saliva as an accessible and sensitive sample type for the detection of respiratory pathogens and host immunity, Lancet Microbe 4 (2023) e837–e850.
[9] G. Choi, T.J. Moehling, R.J. Meagher, Advances in RT-LAMP for COVID-19 testing and diagnosis, Expert Rev. Mol. Diagn. 23 (2023) 9–28.
[10] W. Xiao, et al., CD8 cell counting in whole blood by a paper-based time-resolved fluorescence lateral flow immunoassay, Anal. Chim. Acta 1179 (2021) 10.
[11] Y. Li, et al., Peptide nucleic acid and antifouling peptide based biosensor for the non-fouling detection of COVID-19 nucleic acid in saliva, Biosens. Bioelectron. 225 (2023) 115101.
[12] R. Paul, E. Ostermann, Q. Wei, Advances in point-of-care nucleic acid extraction technologies for rapid diagnosis of human and plant diseases, Biosens. Bioelectron. 169 (2020) 112592.
[13] J. Qian, et al., Rapid and comprehensive detection of viral antibodies and nucleic acids via an acoustofluidic integrated molecular diagnostics chip, AIMDx. Sci. Adv. 11 (2025) eadt5464.
[14] K. Mao, et al., Paper-based microfluidics for rapid diagnostics and drug delivery, J. Control Release 322 (2020) 187–199.
[15] M. Shen, et al., Recent advances and perspectives of nucleic acid detection for coronavirus, J. Pharm. Anal. 10 (2020) 97–101.
[16] A. Bivins, et al., Variability in RT-qPCR assay parameters indicates unreliable SARS-CoV-2 RNA quantification for wastewater surveillance, Water Res. 203 (2021) 117516.
[17] P.B. van Kasteren, et al., Comparison of seven commercial RT-PCR diagnostic kits for COVID-19, J. Clin. Virol. 128 (2020) 104412.
[18] Z. Wei, et al., Isothermal nucleic acid amplification technology for rapid detection of virus, Crit. Rev. Biotechnol. 43 (2023) 415–432.
[19] B. Xiao, et al., Recent advances in centrifugal microfluidic chip-based loop-mediated isothermal amplification, Trends Anal. Chem. 158 (2023) 116836.
[20] Y. Pan, et al., Paper microfluidic sentinel sensors enable rapid and on-site wastewater surveillance in community settings, Cell Rep. Phys. Sci. 5 (2024) 102154.
[21] Y. Yang, et al., Viral and antibody dynamics of acute infection with SARS-CoV-2 omicron variant (B.1.1.529): a prospective cohort study from shenzhen, China, Lancet Microbe 4 (2023) e632–e641.
[22] K.G. Beavis, et al., Evaluation of the EUROIMMUN anti-SARS-CoV-2 ELISA assay for detection of IgA and IgG antibodies, J. Clin. Virol. 129 (2020) 104468.
[23] K. Choi, et al., Digital microfluidics, Annu. Rev. Anal. Chem. 5 (2012) 413–440.
[24] R. Su, F. Wang, M.C. McAlpine, 3D printed microfluidics: advances in strategies, integration, and applications, Lab Chip 23 (2023) 1279–1299.
[25] K. Ren, J. Zhou, H. Wu, Materials for microfluidic chip fabrication, Acc. Chem. Res. 46 (2013) 2396–2406.
[26] H.A. Silva-Neto, et al., Recent advances on paper-based microfluidic devices for bioanalysis, Trends Anal. Chem. 158 (2023) 116893.
[27] J.L. Chen, et al., Advances in microfluidic Paper-Based analytical devices (μPADs): design, fabrication, and applications, Small Methods 8 (2024) 2400155.
[28] Y. Pan, et al., Paper-based devices for rapid diagnosis and wastewater surveillance, Trends Anal. Chem. 157 (2022) 116760.
[29] S. Smith, et al., The potential of paper-based diagnostics to meet the ASSURED criteria, RSC Adv. 8 (2018) 34012–34034.
[30] S. Rink, A.J. Baeumner, Progression of paper-based point-of-care testing toward being an indispensable diagnostic tool in future healthcare, Anal. Chem. 95 (2023) 1785–1793.
[31] V.L. Jamwal, et al., Optimization and validation of RT-LAMP assay for diagnosis of SARS-CoV2 including the globally dominant delta variant, Virol. J. 18 (2021) 178.
[32] C.A.-O.X. Myhrvold, et al., Field-deployable viral diagnostics using CRISPR-Cas13, Science 360 (2018) 444–448.
[33] X. Huang, et al., Developing RT-LAMP assays for rapid diagnosis of SARS-CoV-2 in saliva, EBioMedicine 75 (2022) 103736.
[34] Z. Yang, et al., Rapid veterinary diagnosis of bovine reproductive infectious diseases from semen using Paper-Origami DNA microfluidics, ACS Sens 3 (2018) 403–409.
[35] S. Chojnowska, et al., Human saliva as a diagnostic material, Adv. Med. Sci. 63 (2018) 185–191.
[36] H.Y. Çelebioğlu, S. Lee, I.S. Chronakis, Interactions of salivary mucins and saliva with food proteins: a review, Crit. Rev. Food Sci. Nutr. 60 (2020) 64–83.
[37] A.R. Chandrasekaran, Nuclease resistance of DNA nanostructures, Nat. Rev. Chem. 5 (2021) 225–239.
[38] P.B. Santiago, et al., The pharmacopea within triatomine salivary glands, Trends Parasitol. 36 (2020) 250–265.
[39] Z. Ren, et al., Inhibition of streptococcus mutans polysaccharide synthesis by molecules targeting glycosyltransferase activity, J. Oral. Microbiol 8 (2016) 31095.
[40] S. Kasetsirikul, et al., Detection of the SARS-CoV-2 humanized antibody with paper-based ELISA, Analyst 145 (2020) 7680–7686.
[41] T. Ji, et al., Detection of COVID-19: a review of the current literature and future perspectives, Biosens. Bioelectron. 166 (2020) 112455.
[42] M.N. Aoki, et al., Colorimetric RT-LAMP SARS-CoV-2 diagnostic sensitivity relies on color interpretation and viral load, Sci. Rep. 11 (2021) 9026.
[43] J.L. Davidson, et al., A paper-based colorimetric molecular test for SARS-CoV-2 in saliva, Biosens. Bioelectron. X 9 (2021) 100076.
[44] H.Q. Nguyen, et al., Quantification of colorimetric isothermal amplification on the smartphone and its open-source app for point-of-care pathogen detection, Sci. Rep. 10 (2020) 15123.
[45] T. Zhang, et al., Universally stable and precise CRISPR-LAMP detection platform for precise multiple respiratory tract virus diagnosis including mutant SARS-CoV-2 spike N501, Y. Anal. Chem. 93 (2021) 16184–16193.
[46] M.A. MacMullan, et al., ELISA detection of SARS-CoV-2 antibodies in saliva, Sci. Rep. 10 (2020) 20818.
[47] A.R. Demonbreun, et al., Comparison of IgG and neutralizing antibody responses after one or two doses of COVID-19 mRNA vaccine in previously infected and uninfected individuals, EClinicalMedicine 38 (2021) 101018.
[48] W.N. Chia, et al., Dynamics of SARS-CoV-2 neutralising antibody responses and duration of immunity: a longitudinal study, Lancet Microbe 2 (2021) e240–e249.
[49] J.T. Ladner, et al., Epitope-resolved profiling of the SARS-CoV-2 antibody response identifies cross-reactivity with endemic human coronaviruses, Cell Rep. Med. 2 (2021) 100189.
[50] C.I. Paules, H.D. Marston, A.S. Fauci, Coronavirus infections - more than just the common cold, JAMA 323 (2020) 707–708.
[51] C. Klumpp-Thomas, et al., Standardization of ELISA protocols for serosurveys of the SARS-CoV-2 pandemic using clinical and at-home blood sampling, Nat. Commun. 12 (2021) 113.
[52] A.A.-O. Thomas, et al., Evaluation and deployment of isotype-specific salivary antibody assays for detecting previous SARS-CoV-2 infection in children and adults, Commun. Med. 3 (2023) 37.
[53] S.A.-O. Sciascia, et al., Detection of autoantibodies in saliva as new avenue for the diagnosis and management of autoimmune patients, Diagn. (Basel) 12 (2022) 2026.
[54] F. Mahmoudinobar, D. Britton, J.K. Montclare, Protein-based lateral flow assays for COVID-19 detection, Protein Eng. Des. Sel. 34 (2021) gzab010.
[55] S. Wang, et al., Paper-based chemiluminescence ELISA: Lab-on-paper based on chitosan modified paper device and wax-screen-printing, Biosens. Bioelectron. 31 (2012) 212–218.
[56] G. Wu, J. Srivastava, M.H. Zaman, Stability measurements of antibodies stored on paper, Anal. Biochem. 449 (2014) 147–154.
[57] K.M. Schilling, et al., Fully enclosed microfluidic Paper-Based analytical devices, Anal. Chem. 84 (2012) 1579–1585.
[58] N. Sritong, et al., Development of an integrated sample amplification control for salivary point-of-care pathogen testing, Anal. Chim. Acta 1287 (2024) 342072.
[59] Y. Yan, et al., Rapid and sensitive detection of SARS-CoV-2 based on a phage-displayed scfv antibody fusion with alkaline phosphatase and NanoLuc luciferase, Anal. Chim. Acta 1322 (2024) 343057.
[60] Y. Esteve-Sánchez, et al., SARS-CoV-2 n protein IgG antibody detection employing nanoporous anodized alumina: a rapid and selective alternative for identifying naturally infected individuals in populations vaccinated with spike protein (S)-based vaccines, Sens. Actuators B Chem. 419 (2024) 136378.

Dr. Yuwei Pan earned her Ph.D. from the University of Glasgow (UK), and is a postdoctor at Zhejiang University (China). Her recent research focuses on molecular diagnostics, biosensors, paper-based microfluidic technologies, and wastewater-based epidemiology for public health surveillance, driving interdisciplinary collaborations in key research projects. She has published 9 SCI papers in leading journals, including Cell Reports Physical Science, Trends in Analytical Chemistry, ACS Nano, Biosensors and Bioelectronics, Water Research, and Analytica Chimica Acta, and contributed to three book chapters in environmental science and public health.

Xuanye Ma earned her BSc in Biological Sciences from the University of Leeds (UK) and a second Bachelor's degree in Biology from Xi'an Jiaotong University (China), followed by an MSc in Biosensors from Cranfield University. Her research focuses on developing point-of-care testing (POCT) devices for SARS-CoV-2 detection, combining her interdisciplinary training in biological sciences and biosensor technology to create innovative diagnostic solutions for global health challenges.

Dr. Iva Chianella is Senior Lecturer in Bio-sensors and Functional Polymers within the School of Aerospace, Transport and Manufacturing (SATM) at Cranfield University (UK). After obtaining her first degree in Chemistry from the University of Florence (Italy), Dr Chianella received her PhD in Biosciences from Cranfield University, where she has continued her career as Post-Doctoral Fellow, then Lecturer and she was recently promoted to Senior Lecturer. Dr Chianella main research interests are in the development of chemical and biochemical sensors/nanosensors (electrochemical, optical and piezoelectric) for medical, industrial, environmental, and safety applications; and synthesis of novel polymeric nanomaterials (e.g. Molecularly Imprinted Polymers Nanoparticles) for sensors and assays. Dr Chianella has around 70 publications on the development of sensor/biosensors and on novel polymeric materials and their use in several analytical systems.

Zhugen Yang is a Professor of Biosensing and Environmental Health at Cranfield University, holding a PhD from the University of Lyon and previous positions at the University of Glasgow, Cambridge and Bath. Yang has received several prestigious fellowships, including the Leverhulme Research Leadership Award. His research, focusing on low-cost sensors, has attracted UKRI and industrial funding sources and resulted in more than 100 refereed articles (such as Nature Water) and patents. He is globally recognised for developing an origami paper device for rapid infectious disease diagnosis and sewage testing for COVID-19, part of the UK National Wastewater Surveillance Programme. Yang is an Associate Editor for several journals and has chaired international conferences, driving advancements in environmental sensors and wastewater surveillance. His work has garnered national and international awards (e.g., ACS James Morgan ECR Award) and media recognition, including coverage by the BBC and The Washington Post.

https://dspace.org/

A paper-microfluidic platform for viral RNA and protein detection in saliva for SARS-CoV-2 diagnosis

Pan, Yuwei; Ma, Xuanye; Chianella, Iva; Yang, Zhugen

2026-01-01
Elsevier
https://doi.org/10.1016/j.snb.2025.138731
Pan Y, Ma X, Chianella I, Yang Z. (2026) A paper-microfluidic platform for viral RNA and protein detection in saliva for SARS-CoV-2 diagnosis. Sensors and Actuators B: Chemical, Volume 446, January 2026, Article number 138731

Downloaded from a DSpace repository. https://dspace.org/